Dalton Transactions

PAPER

View Article Online
View Journal | View Issue

Cite this: *Dalton Trans.*, 2018, **47**, 10179

Pt···Pt interaction triggered tuning of circularly polarized luminescence activity in chiral dinuclear platinum(II) complexes†

Xiao-Peng Zhang, *[a] Li-Li Wang,[a] Xiao-Wei Qi,[a] Da-Shuai Zhang,[a] Qian-Ying Yang,[a] Zai-Feng Shi,*[a] Qiang Lin[a] and Tao Wu *[b]

Received 3rd June 2018,
Accepted 28th June 2018

DOI: 10.1039/c8dt02277a

rsc.li/dalton

Circularly polarized luminescence (CPL) activity switched by Pt···Pt interaction is disclosed in two couples of dinuclear Pt(II) complex enantiomers. Upon varying the length of the bridging ligand, intramolecular metal–metal interaction manipulation is achieved as evidenced from crystal structures. Complex (–)-**1** exhibiting strong Pt···Pt interaction displays red phosphorescence with a maximum peak at 638 nm, while complex (–)-**2** exhibiting weak Pt···Pt interaction displays green phosphorescence with a maximum peak at 530 nm. The observed CPL was opposite in sign for the two complexes. TD-DFT simulations further confirmed the influence of the Pt···Pt distance on the difference in the electronic optical activities.

Introduction

Circularly polarized luminescence (CPL) has attracted great interest in the past few decades due to its alluring applications in 3D-displays, enantioselective sensing, optical data storage and bioresponsive imaging.[1] So far, intense CPL emitters are mainly achieved from chiral lanthanide complexes[2] and helical organic molecules.[3] Normally CPL signals can be controlled by perturbing the chiral environment surrounding the luminophores though π–π interactions, hydrogen bonds as well as other intermolecular/intramolecular interactions.[4] In recent years, due to high emission quantum efficiency and tunable excited-state properties, growing attention has been paid to the development of new CPL-active materials focusing on phosphorescent transition metal complexes, such as Ir, Zn, Pt and so on.[5–17]

Among the phosphorescent materials based on transition metal complexes, square-planar Pt(II) complexes are capable of forming self-assemblies, resulting in intriguing luminescent and conductive properties.[18,19] When a chiral substituent is incorporated, the packing of adjacent units adopts a staggered pattern alongside the Pt···Pt chain due to steric hindrance, which is favourable for forming a helical supramolecular structure. The helical structure may exhibit a significant difference in the magnetic dipole transition from the excited triplet state to the ground state, which can show interesting CPL activity.[14–17] Through incorporation of a helical fragment or heterobidentate *trans*-spanning blocks, distinctive CPL signals can also be accessed in Pt(II) complexes,[10–12] some of which have been exploited to fabricate circularly polarized phosphorescent organic light-emitting diodes (CP-PHOLEDs) with a good brightness and a sizable dissymmetry factor (g_{lum}, defined as: $g_{lum} = 2(I_L - I_R)/(I_L + I_R)$ where I_L and I_R are the left- and right- circularly polarized intensity, respectively).[13]

Recently, studies on vapor-, solvent-, mechano-, and temperature-induced structural and chiroptical switches of cyclometalated Pt(II) complexes[17,20] indicated that CPL activity can be reasonably tuned by the manipulation of temperature and solvent.[17] However, studies on the CPL of Pt(II) complex monomer emission are rare, and many points such as the impact of Pt···Pt interaction on the CPL activity of chiral Pt(II) complexes are not understood yet.

In the present study, we prepared two couples of dinuclear Pt(II) complexes, [(–)-(C^N^N)Pt]$_2$dppmCl$_2$ (–)-**1** ((–)-(C^N^N) = (–)-4,5-pinene-6′-phenyl-2,2′-bipyridine) and [(+)-(C^N^N)Pt]$_2$dppmCl$_2$ (+)-**1** ((+)-(C^N^N) = (+)-4,5-pinene-6′-phenyl-2,2′-bipyridine) linked by bis(diphenylphosphino)methane (dppm), and [(–)-(C^N^N)Pt]$_2$dppeCl$_2$ (–)-**2** and [(+)-(C^N^N)Pt]$_2$dppeCl$_2$ (+)-**2** linked by bis(diphenylphosphino)ethane (dppe) (Scheme 1), and investigated their CPL to understand the influence of Pt···Pt interaction on the optical activity in the excited state.

[a]*Key Laboratory of Water Pollution Treatment & Resource Reuse of Hainan Province, College of Chemistry and Chemical Engineering, Hainan Normal University, Haikou 571158, People's Republic of China. E-mail: zxp_inorganic@126.com, zaifengshi_hnnu@sina.com*

[b]*Institute of Organic Chemistry and Biochemistry, Academy of Sciences, Flemingovo náměstí 2, 16610 Prague 6, Czech Republic. E-mail: wu@uochb.cas.cz*

†Electronic supplementary information (ESI) available: Experimental methods, the preparation of complexes, crystallographic data, spectroscopic data and theoretical calculation details (PDF). CCDC 1830652 ((+)-**1**), 1830653 ((–)-**2**-ClO$_4$-Cl), and 1830654 ((–)-**1**). For ESI and crystallographic data in CIF or other electronic format see DOI: 10.1039/c8dt02277a

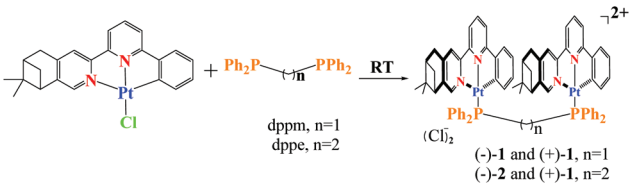

Scheme 1 Synthesis route of chiral dinuclear Pt(II) complexes (−)-**1**, (+)-**1**, (−)-**2** and (+)-**2**.

Experimental section

General methods

All reagents were purchased from commercial suppliers and used as received (**Caution**: Perchlorates are potentially explosive and must be handled with great care and in small amounts. Collision and friction must be avoided.) Mass spectra were acquired on an LCQ Fleet ESI Mass Spectrometer. The NMR spectra were obtained on a Bruker DRX-500 spectrometer. Coupling constants are given in hertz. UV-Vis spectra were measured on a UV-3600 spectrophotometer. Elemental analysis was performed on a PerkinElmer 240C analyzer. Photoluminescence (PL) spectra were measured by using a Hitachi F-4600 PL spectrophotometer (λ_{ex} = 420 nm). Luminescent quantum yields and lifetimes were measured on a HORIBA JY system. The electronic circular dichroism (ECD) spectra in CH_2Cl_2 solution were recorded on a Jasco J-810 spectropolarimeter (using a 10 mm quartz cell for a concentration of 5×10^{-5} mol L^{-1}). The CPL spectra were recorded using a circular polarizer on a Jasco CPL-300 spectrophotometer at a scan rate of 100 nm min^{-1} and 1 nm resolution at room temperature (using a 10 mm quartz cell for a concentration of 5×10^{-5} mol L^{-1}). Mononuclear complexes (−)-(C^N^N)PtCl and (+)-(C^N^N)PtCl were prepared according to a previous method.[20] Compounds (+)-**1** and (+)-**2** were obtained using the same procedures as for (−)-**1** and (−)-**2**, respectively.

Synthesis of [(−)-(C^N^N)Pt]$_2$dppmCl$_2$, (−)-1

A mixture of (−)-(C^N^N)PtCl (334 mg, 0.60 mmol) and bis (diphenylphosphino)methane (dppm) (115 mg, 0.30 mmol) was stirred in a CH_2Cl_2/CH_3OH (30/10 mL) solution at room temperature under an argon atmosphere. After stirring for 12 hours, the resultant solution was evaporated under reduced pressure, and red powders were obtained. The red crystallites can be isolated by recrystallization in a chloroform solution (80%). MS (ESI) (m/z): $[M]^{2+}$ calcd for $C_{71}H_{64}N_4P_2Pt_2$, 712.2; found, 712.4. Anal. calcd for $C_{71}H_{64}N_4P_2Pt_2Cl_2$ ((−)-**1**): C, 56.99; H, 4.31; N, 3.74%. Found: C, 56.96; H, 4.27; N, 3.73%. ^{1}H NMR (500 MHz, DMSO-d6, 295 K): δ 8.42 (m, 3H), 8.38 (m, 3H), 8.06 (s, 2H), 8.02 (t, J = 8.0 Hz, 2H), 7.93(d, J = 8.0 Hz, 2H), 7.76 (d, J = 8.0 Hz, 3H), 7.66 (m, 2H), 7.55 (t, J = 6.5 Hz, 4H), 7.48 (t, J = 7.0 Hz, 4H), 7.42 (m, 3H), 7.17 (d, J = 7.5 Hz, 2H), 6.77 (d, J = 7.0 Hz, 2H), 6.61 (t, J = 7.5 Hz, 2H), 6.52 (d, J = 7.5 Hz, 2H), 5.15 (t, J = 12.0 Hz, 2H), 3.11 (d, J = 17.5 Hz, 2H), 2.82 (d, J = 17.5 Hz, 2H), 2.61–2.64 (m, 2H), 2.19 (m, 2H), 1.39 (t, J = 5.0 Hz, 2H), 1.26 (s, 6H), 1.24 (d, J = 9.5 Hz, 2H), 0.29 (s, 6H). ^{13}C NMR (125 MHz, DMSO-d6, 295 K): δ 161.8, 154.3, 153.2, 149.6, 146.8, 146.4, 145.7, 142.3, 137.9, 133.8, 133.4, 133.2, 132.9, 131.8, 131.2, 130.3, 129.5, 129.0, 125.8, 125.2, 123.4, 119.7, 119.6, 79.3, 44.6, 38.3, 38.2, 32.7, 30.9, 25.5, 20.9. ^{31}P NMR (202 MHz, DMSO-d6, 295 K): δ 20.51 ($^1J_{PtP}$ = 4111 Hz).

Synthesis of [(−)-(C^N^N)Pt]$_2$dppeCl$_2$, (−)-2

A mixture of (−)-(C^N^N)PtCl (334 mg, 0.60 mmol) and bis (diphenylphosphino)ethane (dppe) (120 mg, 0.30 mmol) was stirred in a CH_2Cl_2/CH_3OH (30/10 mL) solution at room temperature under an argon atmosphere. After stirring for 12 hours, the solvent was removed under reduced pressure. The residue was washed with chloroform and *n*-hexane, and green-yellow powders were obtained (60%). MS (ESI) (m/z): $[M]^{2+}$ calcd for $C_{72}H_{66}N_4P_2Pt_2$, 719.7; found, 719.3. Anal. calcd for $C_{72}H_{66}N_4P_2Pt_2Cl_2$ ((−)-**2**): C, 57.26; H, 4.40; N, 3.71%. Found: C, 57.24; H, 4.39; N, 3.68%. ^{1}H NMR (500 MHz, DMSO-d6, 295 K): δ 8.02–8.12 (m, 8H), 8.00 (t, J = 8.0 Hz, 3H), 7.89 (m, 3H), 7.70 (d, J = 8.0 Hz, 2H), 7.45–7.50 (m, 6H), 7.41 (m, 6H), 7.05 (d, J = 8.0 Hz, 2H), 6.51 (t, J = 7.5 Hz, 2H), 5.91–6.05 (m, 6H), 3.71–4.07 (m, 4H), 3.09 (d, J = 17.5 Hz, 2H), 2.91 (d, J = 18.0 Hz, 2H), 2.61–2.65 (m, 2H), 2.23 (m, 2H), 1.79 (m, 2H), 1.30 (s, 6H), 1.07 (m, 2H), 0.37 (s, 6H). ^{13}C NMR (125 MHz, DMSO-d6, 295 K): δ 161.8, 155.7, 153.3, 149.7, 147.3, 146.4, 146.2, 142.1, 136.9, 134.9, 132.9, 132.1, 131.5, 131.2, 130.3, 129.8, 129.4, 129.0, 125.4, 125.0, 124.0, 119.8, 119.6, 56.0, 44.5, 38.7, 38.4, 32.6, 30.5, 25.4, 20.8. ^{31}P NMR (202 MHz, DMSO-d6, 295 K): δ 19.21 ($^1J_{PtP}$ = 4093 Hz).

Single crystal X-ray structure determination

Red crystals of complexes (−)-**1** and (+)-**1** suitable for X-ray analysis were isolated by recrystallization in the chloroform solution at 273 K. Green-yellow crystals of ([(+)-(C^N^N)Pt]$_2$dppe)$_2$(ClO_4)$_3$Cl suitable for X-ray analysis were obtained by the replacement of Cl with a ClO_4 anion. An aqueous solution (10 mL) of silver perchlorate (33.2 mg, 0.16 mmol) was added into a 20 mL dichloromethane solution of (−)-**2** (151 mg, 0.10 mmol) for 30 min, and then the separated organic phase was evaporated and recrystallized in a mixed solvent of acetonitrile/acetone (v/v = 3 : 1).

Single-crystal X-ray diffraction measurements were carried out on a Bruker SMART APEX CCD based on a diffractometer operating at room temperature. Intensities were collected with graphite monochromatized Mo Kα radiation (λ = 0.71073 Å) operating at 50 kV and 30 mA, using $\omega/2\theta$ scan mode. Data reduction was made with the Bruker SAINT package.[27] Absorption corrections were performed using the SADABS program.[28] The structures were solved by direct methods and refined on F^2 by full-matrix least-squares using SHELXL-97 with anisotropic displacement parameters for all non-hydrogen atoms in the two structures. Hydrogen atoms bonded to the carbon atoms were placed in calculated positions and refined as riding mode, with C–H = 0.93 Å (methane) or 0.96 Å (methyl) and U_{iso}(H) = 1.2 U_{eq} ($C_{methane}$) or U_{iso}(H) = 1.5 U_{eq} (C_{methyl}). The water hydrogen atoms were located in the differ-

ence Fourier maps and refined with an O–H distance restraint [0.85(1) Å] and U_{iso}(H) = 1.5 U_{eq}(O). All computations were carried out using the SHELXTL-97 program package.[29] CCDC 1830652–1830654† contain the supplementary crystallographic data for this paper.

Calculation methods

Crystal structures of the Pt complexes were used as the starting geometry and optimization was performed using the Gaussian09 program.[30] The CAM-B3LYP functional, SVP basis set for C, H, N, and P, MWB60 pseudopotential basis set for Pt, and the conductor-like polarizable continuum solvent model (CPCM) were used.[31] TD-DFT simulations were performed with the same functional and basis sets. The calculated ECD spectrum was drawn by using the software SpecDis,[32] in which the sigma per eV was set at 0.2.

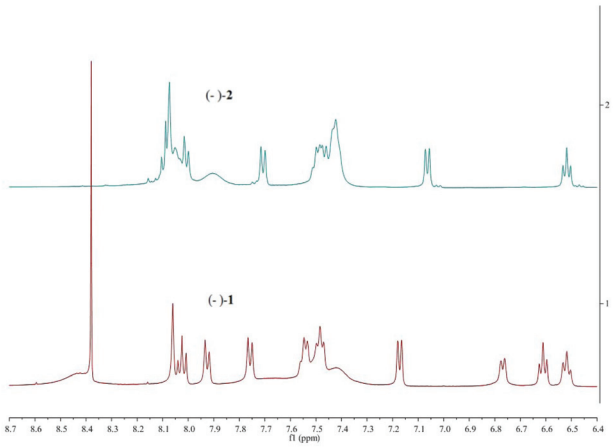

Fig. 1 ^{1}H NMR spectra of (–)-**1** and (–)-**2** in the region of δ 6.4–8.7 ppm.

Results and discussion

Synthesis and characterization

Pinene derived cyclometalating ligands and mononuclear precursor were synthesized on the basis of a previous procedure.[20] The dinuclear complexes **1** and **2** are easily obtained in moderate yields by the reaction of the mononuclear enantiomeric complexes with two diphosphines. NMR spectra of complexes (–)-**1** and (–)-**2** in solution are listed in Fig. S1–S16.† There are several apparent spectral differences between the ^{1}H NMR spectra of complexes (–)-**1** and (–)-**2**. For example, the chemical shift of group –C*H*$_3$ in the pinene skeleton was observed at *ca.* 0.29 and 1.26 ppm in (–)-**1** (Fig. S1†), while it moved to 0.37 and 1.30 ppm in (–)-**2** (Fig. S9†). The most characteristic variance is the chemical shift between the two bridge units, *i.e.* PCH$_2$P in (–)-**1** (5.15 (t, J = 12.0 Hz, 2H); see Fig. S1,† S5 & S6) and PCH$_2$CH$_2$P in (–)-**2** (3.71–4.07 (m, 4H); see Fig. S9, S13 & S14†).[23] The former is similar to the case in which metal–metal interactions are strong between the two platinum atoms in solution,[23a] while the latter is more likely related to weak metal–metal interactions between the two platinum atoms.[23b] Other differences were also observed on the hydrogens from the aromatic rings (Fig. 1); one distinctive signal is observed at downfield (δ 8.42, 8.38 ppm) in (–)-**1** exclusively (Fig. 1), which is similar to that of the monomeric precursor,[20a] probably arising from the atoms close to the two Pt cores.[23b] Both the ^{1}H and ^{1}H–^{1}H NOESY NMR spectra of (–)-**1** (Fig. S1 & S8†) and (–)-**2** (Fig. S9 & S16†) indicated that the signal of protons on 6′-phenyl-2,2′-bipyridine are down-shifted in **1**, which is similar to that of other binuclear platinum(II) complexes.[23b]

Crystal structures and Pt···Pt distances

The red crystal of complex (–)-**1** suitable for X-ray analysis was obtained from a CHCl$_3$ solution. The green-yellow crystal of (–)-**2** was obtained by counterion metathesis, where part of the Cl$^-$ anions was substituted by ClO$_4^-$. Complex (–)-**1** crystallizes in the $P2_12_12_1$ space group of an orthorhombic system with one [(–)-(C^N^N)Pt]$_2$dppm^{2+} cation in the asymmetrical unit, while (–)-**2** falls in the $P2_1$ space group of a monoclinic system (Table 1, Fig. 2). Two [(+)-(C^N^N)Pt]$_2$dppe^{2+} cations and three ClO$_4^-$ and one Cl$^-$ anions are involved in the asymmetrical unit of (–)-**2**. The bond distances and bond angles surrounding the Pt(II) core in (–)-**1** and (–)-**2** are similar to previously reported data of analogous Pt(II) complexes (Table S1†).[21–24] In the crystal structure of (–)-**1**, two [(–)-(C^N^N)Pt]$^+$ moieties displaying almost identical square-planar geometry are bridged by the dppm ligand, and they are staggered along the Pt–Pt axis with a torsion angle θ of 29.24° (defined by the angle between the Pt1–Pt2–N1 and Pt1–Pt2–N3 planes). As expected, the structure of complex (+)-**1** appears almost as a mirror-image of that of (–)-**1** (Fig. S17†). Despite the steric hindrance of the pinene group, the staggered arrangement in (–)-**1** facilitates an appreciable intramolecular Pt···Pt interaction (3.10 Å) that falls within the range (3.09–3.50 Å) predicted for effective metal–metal interactions.[21–24] In contrast, the intermolecular Pt···Pt distance between two nearest discrete [(–)-(C^N^N)Pt]$_2$dppm^{2+} units is 16.20 Å, which excludes any effective intermolecular interaction (Fig. S18†).

As for complex (–)-**2**, because of the flexible conformation of dppe, two [(–)-(C^N^N)Pt]$_2$dppe^{2+} cations in the asymmetrical unit of the complex adopts different arrangements with dissimilar torsion angles θ as 23.92° (defined by the angle between the Pt3–Pt4–N1C and Pt3–Pt4–N1D planes) and 27.25° (defined by the angle between the Pt1–Pt2–N1A and Pt1–Pt2–N1B planes). Unlike dppm in complex (–)-**1**, the longer bridging ligand dppe in complex (–)-**2** prohibits close contact between two [(–)-(C^N^N)Pt]$^+$ units. The intramolecular Pt–Pt distances are 3.67 and 4.09 Å, which indicates the absence of an effective intramolecular Pt···Pt interaction in (–)-**2**. Furthermore, there is no valid intermolecular Pt···Pt interaction (Fig. S19†).

Electronic absorption and emission spectra

Both complexes (–)-**1** and (–)-**2** display characteristic absorption bands (ε > 10^4 L mol^{-1} cm^{-1}) in the UV region normally

Table 1 Crystallographic data of (−)-**1**, (+)-**1** and (−)-**2**-ClO_4-Cl

	(−)-**1**	(+)-**1**	(−)-**2**-ClO_4-Cl
Formula	$C_{74}H_{71}Cl_{11}N_4O_2P_2Pt_2$	$C_{74}H_{71}Cl_{11}N_4O_2P_2Pt_2$	$C_{154}H_{149}Cl_4N_{13}O_{13}P_4Pt_4$
M_r/g mol^{-1}	1890.41	1890.41	3435.89
Crystal system	Orthorhombic	Orthorhombic	Monoclinic
Space group	$P2_12_12_1$	$P2_12_12_1$	$P2_1$
a/Å	17.8626(6)	17.8378(9)	14.5011(11)
b/Å	18.8915(6)	18.8895(8)	22.6547(17)
c/Å	22.3609(6)	22.3559(10)	23.2331(18)
α/°	90.00	90.00	90.00
β/°	90.00	90.00	103.3760(10)
γ/°	90.00	90.00	90.00
V/Å^3	7545.7(4)	7532.7(6)	7425.4(10)
Z	4	4	2
T/K	293(2)	293(2)	296(2)
Radiation, λ/Å	0.71073	0.71073	0.71073
D_{calcd}, g cm^{-3}	1.664	1.667	1.537
μ/mm^{-1}	4.183	4.191	3.935
F(000)	3728	3728	3416
Crystal size/mm^3	0.28 × 0.26 × 0.20	0.30 × 0.24 × 0.22	0.38 × 0.35 × 0.29
θ range/°	2.280 to 25.000	2.284 to 25.999	0.901 to 27.496
Reflections measured	27 064	27 665	66 584
Unique reflections	12 938	14 116	30 659
R_{int}	0.0438	0.0453	0.0537
Reflections with $F^2 > 2\sigma(F^2)$	10 821	11 606	27 710
Number of parameters	860	860	1695
Goodness-of-fit on F^2	1.002	1.001	1.041
R_1 [$F^2 > 2\sigma(F^2)$]	0.0434	0.0404	0.0432
wR_2 (all data)	0.0946	0.0893	0.1069
$\Delta\rho_{max}$, $\Delta\rho_{min}$/e Å^{-3}	0.981, −0.738	1.026, −0.754	1.888, −2.917
Flack parameter	−0.017(5)	−0.014(4)	0.030(4)

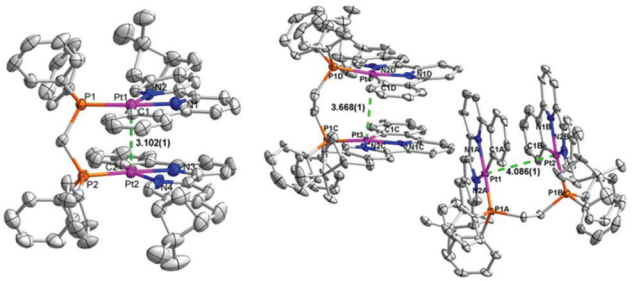

Fig. 2 Perspective view of the cations of (−)-**1** (left) and (−)-**2**-ClO_4-Cl (right). H atoms and solvent molecules are omitted for clarity.

as that of bis-(diphenylphosphino)alkane bridged dinuclear Pt(II) complexes (Fig. 3, 4 and Table S2†). The strongest bands (<400 nm) are assigned to intraligand π–π* transitions. The broad absorption at 400–450 nm is ascribed to a mixture of metal-to-ligand charge transfer (^{1}MLCT) and ligand-to-ligand charge transfer (^{1}LLCT) transitions. In particular, the weak absorption in the region of 470–550 nm (^{1}MMLCT, metal–metal-to-ligand charge transfer transition) in complex (−)-**1** is contributed by the effective intramolecular Pt···Pt interaction.[21–24] For complex (−)-**2**, there is almost no signal in this spectral range, indicating that the metal–metal interactions between the two Pt centers are negligible.

A correlation between emission and temperature is plotted in Fig. S20.† At lower temperatures, the emission spectra of both complex (−)-**1** and (−)-**2** are blue-shifted, and the bands are slimmer. For complex (−)-**2**, the spectral resolution at lower temperatures is significantly enhanced (Table S2†), while complex (−)-**1** exhibits a structureless broad emission band.[21–24] It is interesting to note that the luminescence color shifts from red phosphorescence (complex (−)-**1**, with an emission maximum peak at 638 nm) to green phosphorescence (complex (−)-**2**, with an emission maximum peak at 530 nm) as the Pt···Pt distance shortens. The emission spectrum of (−)-**2** exhibits a vibronic-structure with a progression spacing of approximately 1100 cm^{-1} (Fig. 4), which is characteristic of the skeletal stretching of the free C^N^N ligand, clearly indicating the involvement of the C^N^N ligand in the excited state.[21–24]

In a dichloromethane solution, the emission spectrum of complex (−)-**2** displays less difference than that of (−)-**1** if compared to the spectrum of their mononuclear precursor (−)-(C^N^N)PtCl (Fig. S21†). Obviously, a shorter distance between the two [(C^N^N)Pt] units in (−)-**1** is more favorable for various intramolecular interactions that leads to the red-shift in emission. Similar to the absorption spectra, the emission also displays the influence of distance and interactions between the two [(C^N^N)Pt] units. The high-energy emission at 530 nm in (−)-**2** is assigned to the ^{3}MLCT state similar to that of a mononuclear chloroplatinum(II) precursor complex, indicating that the two [(C^N^N)Pt] units manifest as almost discrete blocks. The low-energy emission at 638 nm in (−)-**1** is attributed to the ^{3}MMLCT state owing to the short distance and interactions between the two platinum atoms.[21–24]

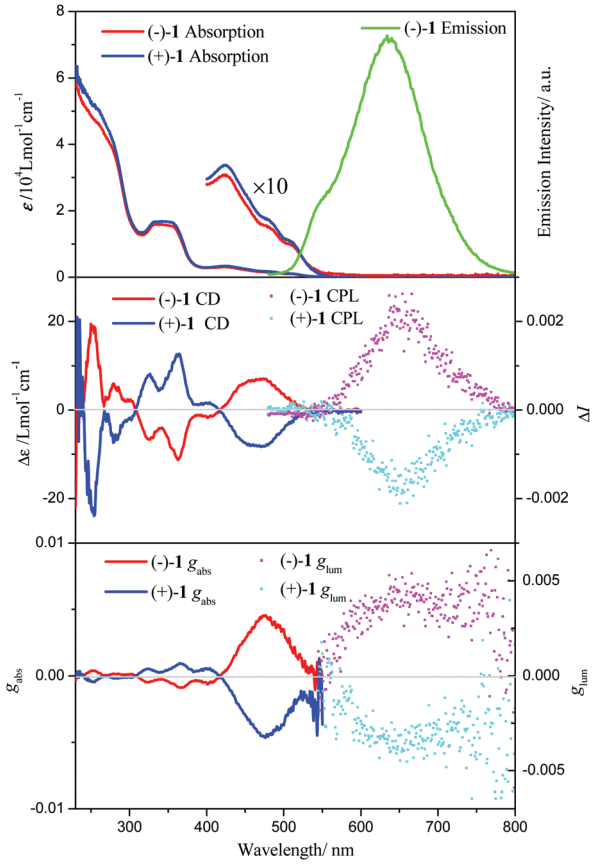

Fig. 3 Absorption spectra of (–)-**1** and (+)-**1** and emission spectrum of (–)-**1** in CH_2Cl_2 (5×10^{-5} mol L^{-1}) at T = 298 K, λ_{ex} = 420 nm (top); ECD and CPL spectra of (–)-**1** and (+)-**1** in CH_2Cl_2 (5×10^{-5} mol L^{-1}) at T = 298 K (middle); g_{abs} and g_{lum} factors of (–)-**1** and (+)-**1** (bottom).

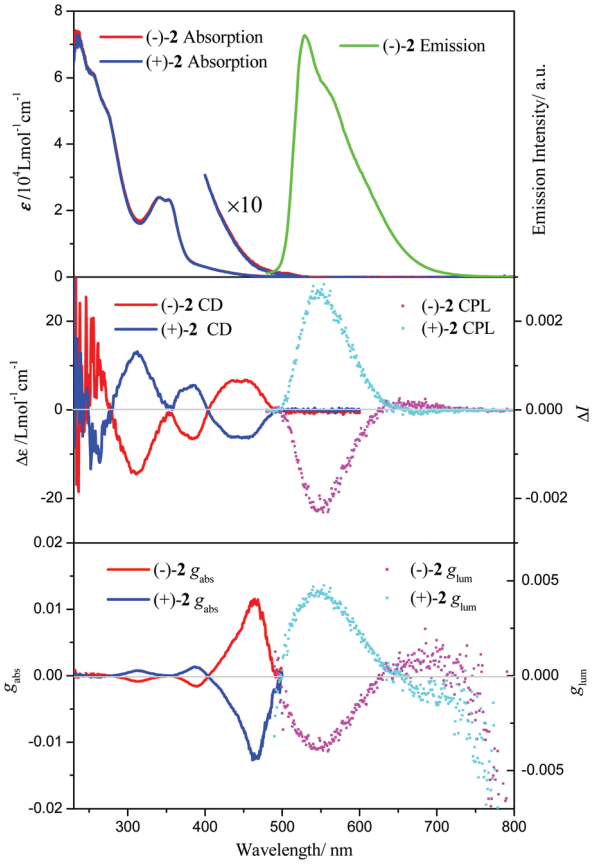

Fig. 4 Absorption spectra of (–)-**2** and (+)-**2** and emission spectrum of (–)-**2** in CH_2Cl_2 (5×10^{-5} mol L^{-1}) at T = 298 K, λ_{ex} = 420 nm (top); CD and CPL spectra of (–)-**2** and (+)-**2** in CH_2Cl_2 (5×10^{-5} mol L^{-1}) at T = 298 K (middle); g_{abs} and g_{lum} factors of (–)-**2** and (+)-**2** (bottom).

Solvent dependent emission and excitation spectra of (–)-**1** (Fig. S22†) and (–)-**2** (Fig. S23†) were further measured to evaluate the influence of solvent polarity on the extent of metal–metal interactions.[25,26] It can be found that the emission spectra of (–)-**1** are more sensitive than those of (–)-**2** to polarity due to the variation of Pt⋯Pt contacts in different solvents. In contrast, the solution emission maximum of (–)-**2** presents minimal changes in different solvents.

Chiroptical properties

The electronic optical activity (ECD (electronic circular dichroism) and CPL) properties of complexes (–)-**1** and (–)-**2** are plotted in Fig. 3 and 4, respectively. The ECD spectrum of (–)-**1** shows many bands in the region of 240–500 nm (positive: 253, 280 and 465 nm; negative: 325, 363 and 400 nm) in a CH_2Cl_2 solution, while the ECD spectrum of (–)-**2** shows fewer bands (positive: 256 and 445 nm; negative: 310 and 381 nm). The maximum values of the dissymmetry factor g (defined as: $g = \Delta\varepsilon/\varepsilon$) are significantly different for complexes (–)-**1** (4.5×10^{-3} at 475 nm) and (–)-**2** (1.1×10^{-2} at 465 nm), which indicates that metal–metal interactions play a key role in the variance of optical activity in the ground state. The strong Pt⋯Pt interaction in (–)-**1** increases the rigidity of its geometry, and the exciton coupling between the two [(C^N^N)Pt] units is less efficient than that in (–)-**2**.[2b]

The most interesting phenomenon is the optical activity of these two complexes in the excited state. As expected, the CPL spectra of complexes (–)-**1** and (–)-**2** appeared as almost mirror-images of their enantiomers (+)-**1** and (+)-**2** (Fig. 3 and 4). Unlike the big difference in the values of the dissymmetry factor in the ground state between complexes (–)-**1** and (–)-**2**, the values of the dissymmetry factor in the excited state between complexes (–)-**1** and (–)-**2** (around the maximum emission band, 640 nm for (–)-**1** and 550 nm for (–)-**2**) are quite close. Meanwhile, the g_{lum} values are similar to those of the reported cases for helicene derived Pt(II) complexes or square-planar Pt(II) complexes with helical structures.[10–17] Due to the short distance and interactions between the two platinum centers, the CPL bands of complex (–)-**1** are dominated by the dimeric excited state ^{3}MMLCT. For complex (–)-**2**, the CPL bands mainly come from monomeric excited state ^{3}MLCT.[17]

Note that the conformation of the bridging ligand dppe is more flexible than that of dppm, where the two [(C^N^N)Pt] units can rotate along the linked oligophosphine axis. Thus the distance and interactions between the two platinum

centers in complex (−)-**2** may be shorter in solution than those in the crystal.[21–24] According to studies by Shinozaki and co-workers,[15] the difference of dihedral angles between the two [(C^N^N)Pt] units can profoundly influence the values of oscillator strength and rotatory strength. This is probably responsible for the opposite CPL signs in (−)-**1** and (−)-**2**.

DFT calculation

Besides the difference in the values of the dissymmetry factor, most of the ECD bands between complexes (−)-**1** and (−)-**2** are relatively similar since they are almost dominated by the ground electronic states of the mononuclear $[(-)\text{-}(C^N^N)Pt]^+$ unit. The Pt cores share almost similar square-planar geometry in the structures of both complexes (−)-**1** and (−)-**2**, which almost coincides with the TDDFT calculated data (Fig. 5 and 6).

A comparison of the Pt···Pt distances of Pt(II) complexes (−)-**1** and (−)-**2** between optimized and crystal structures are listed in Table 2, and the HOMO and LUMO orbitals of the two complexes are plotted in Fig. 7. Although there is some discrepancy between simulated and crystal structures, it is apparent that the Pt···Pt distance in complex (−)-**1** is much shorter than that in (−)-**2**, which produces a distinctive difference in their optical activities in the excited states. The optimized Pt···Pt separation of complex (−)-**2** is 3.50 Å, which falls on the border of the scope of intermetal distances (3.09–3.50 Å), indicating that weak metal–metal interactions between the two Pt atoms in solution might be possible. The weak interactions are probably responsible for the weak CPL band observed around 690 nm.[17]

The HOMO/LUMO of (−)-**1** and (−)-**2** having $\theta = 10.7°$ (Fig. 7 upper, angle between the Pt1–Pt2–N1 and Pt1–Pt2–N3 planes) and $\theta = 6.7°$ (Fig. 7 lower), respectively, which are much smaller compared to those in their crystal structures ($\theta = 29.24°$ for (−)-**1** and $\theta = 23.92°$ for (−)-**2**). The HOMO of complex (−)-**1** exhibits strong bonding orbitals between the two Pt centers. Apparent bonding orbitals between the two aromatic planes are also visible. For the HOMO of complex (−)-**2**, weak bonding orbitals between the two Pt centers can be visualized; however, there are no obvious bonding orbitals between the two aromatic planes. The LUMO in both complexes are almost dominated by the π^* orbital of two aromatic planes.

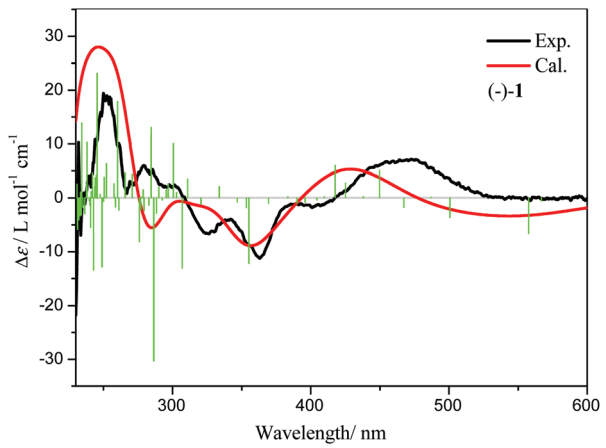

Fig. 5 Simulated rotatory strength (green) and ECD spectrum (red) of complex (−)-**1** in dichloromethane solution in comparison with its experimental values (black).

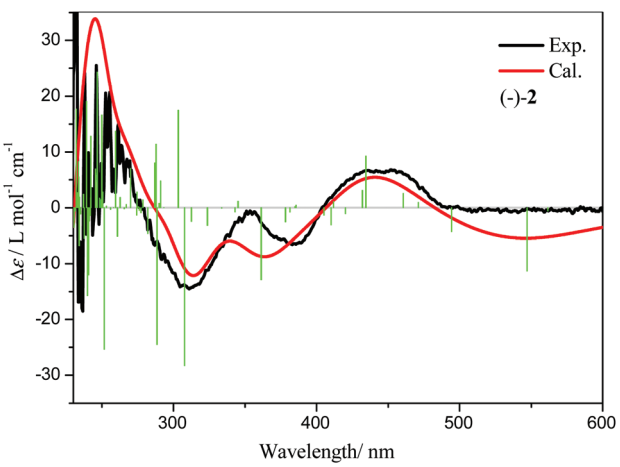

Fig. 6 Simulated rotatory strength (green) and ECD spectrum (red) of complex (−)-**2** in dichloromethane solution in comparison with its experimental values (black).

Table 2 Comparison of Pt···Pt distances of complexes (−)-**1** and (−)-**2** in the crystalline state and CAM-B3LYP functional optimized geometries in dichloromethane solution

	Pt···Pt distance	
Complex	Crystal	Optimized
(−)-**1**	310.2 pm	320.6 pm
(−)-**2**	366.8 pm	350.1 pm

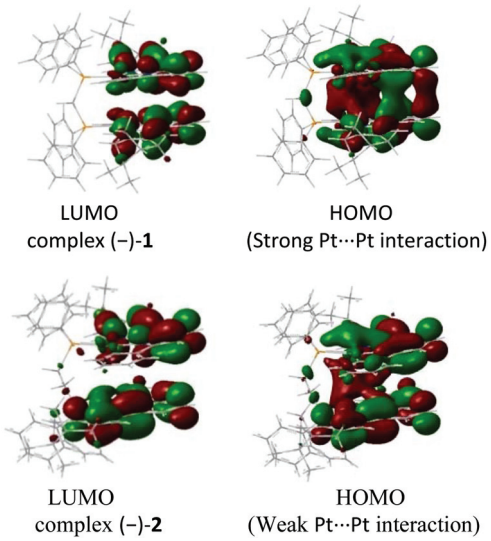

Fig. 7 Selected molecular orbitals of complexes (−)-**1** (upper) and (−)-**2** (lower).

Conclusions

We have obtained two couples of chiral dinuclear Pt(II) complexes displaying different Pt···Pt interactions by choosing bridging ligands with different lengths, which was straightforwardly in the crystal structure determined by single crystal X-ray crystallography. Not only the shift of the luminescence color, but also the inversion of the sign of CPL activity was observed. The results manifest the importance of CPL spectroscopy in the study of metal–metal interactions, which are likely to facilitate the development of rationally designed chiral materials.

Conflicts of interest

There are no conflicts to declare.

Acknowledgements

This work was supported by the National Natural Science Foundation of China (21601043), Natural Science Foundation of Hainan Province (217100, 217101, ZDYF2017011, ZDKJ2016022-02 and 2017CXTD007), and Grantová Agentura České Republiky (16-08764Y).

Notes and references

1 (*a*) C. Wagenknecht, C.-M. Li, A. Reingruber, X.-H. Bao, A. Goebel, Y.-A. Chen, Q. Zhang, K. Chen and J.-W. Pan, *Nat. Photonics*, 2010, **4**, 549–552; (*b*) R. Carr, N. H. Evans and D. Parker, *Chem. Soc. Rev.*, 2012, **41**, 7673–7686; (*c*) Y. Yang, R. C. da Costa, M. J. Fuchter and A. J. Campbell, *Nat. Photonics*, 2013, **7**, 634–638; (*d*) T. Wu and P. Bouř, *Chem. Commun.*, 2018, **54**, 1790–1792.

2 (*a*) F. Zinna, U. Giovanella and L. Di Bari, *Adv. Mater.*, 2015, **27**, 1791–1795; (*b*) T. Wu, X.-Z. You and P. Bouř, *Coord. Chem. Rev.*, 2015, **284**, 1–18; (*c*) T. Wu, J. Kapitán, V. Mašek and P. Bouř, *Angew. Chem., Int. Ed.*, 2015, **54**, 14933–14936; (*d*) C.-T. Yeung, K.-H. Yim, H.-Y. Wong, R. Pal, W.-S. Lo, S.-C. Yan, M. Y.-M. Wong, D. Yufit, D. E. Smiles, L. J. McCormick, S. J. Teat, D. K. Shuh, W.-T. Wong and G.-L. Law, *Nat. Commun.*, 2017, **8**, 1128; (*e*) G. Muller, *Dalton Trans.*, 2009, **38**, 9692–9707; (*f*) R. Carr, N. H. Evans and D. Parker, *Chem. Soc. Rev.*, 2012, **41**, 7673–7686.

3 (*a*) I. H. Delgado, S. Pascal, A. Wallabregue, R. Duwald, C. Besnard, L. Guénée, C. Nançoz, E. Vauthey, R. C. Tovar, J. L. Lunkley, G. Muller and J. Lacour, *Chem. Sci.*, 2016, **7**, 4685–4693; (*b*) J. Zhang, W. Feng, H. Zhang, Z. Wang, H. A. Calcaterra, B. Yeom, P. A. Hu and N. A. Kotov, *Nat. Commun.*, 2016, **7**, 10701; (*c*) D. Yang, P. Duan, L. Zhang and M. Liu, *Nat. Commun.*, 2017, **8**, 15727.

4 (*a*) M. Liu, L. Zhang and T. Wang, *Chem. Rev.*, 2015, **115**, 7304–7397; (*b*) J. F. Kögel, S. Kusaka, R. Sakamoto, T. Iwashima, M. Tsuchiya, R. Toyoda, R. Matsuoka, T. Tsukamoto, J. Yuasa, Y. Kitagawa, T. Kawai and H. Nishihara, *Angew. Chem., Int. Ed.*, 2016, **55**, 1377–1381; (*c*) S. Ito, K. Ikeda, S. Nakanishi, Y. Imai and M. Asami, *Chem. Commun.*, 2017, **53**, 6323–6326.

5 C. Schaffner-Hamann, A. von Zelewsky, A. Barbieri, F. Barigelletti, G. Muller, J. P. Riehl and A. Neels, *J. Am. Chem. Soc.*, 2004, **126**, 9339–9348.

6 K. D. Oyler, F. J. Coughlin and S. Bernhard, *J. Am. Chem. Soc.*, 2007, **129**, 210–217.

7 T.-Y. Li, Y.-M. Jing, X. Liu, Y. Zhao, L. Shi, Z. Tang, Y.-X. Zheng and J.-L. Zuo, *Sci. Rep.*, 2015, **5**, 14912.

8 N. Hellou, M. Srebro-Hooper, L. Favereau, F. Zinna, E. Caytan, L. Toupet, V. Dorcet, M. Jean, N. Vanthuyne, J. A. G. Williams, L. Di Bari, J. Autschbach and J. Crassous, *Angew. Chem., Int. Ed.*, 2017, **56**, 8236–8239.

9 R. Aoki, R. Toyoda, J. F. Kögel, R. Sakamoto, J. Kumar, Y. Kitagawa, K. Harano, T. Kawai and H. Nishihara, *J. Am. Chem. Soc.*, 2017, **139**, 16024–16027.

10 C. Shen, E. Anger, M. Srebro, N. Vanthuyne, K. K. Deol, T. D. Jefferson Jr., G. Muller, J. A. G. Williams, L. Toupet, C. Roussel, J. Autschbach, R. Réau and J. Crassous, *Chem. Sci.*, 2014, **5**, 1915–1927.

11 T. Biet, T. Cauchy, Q. Sun, J. Ding, A. Hauser, P. Oulevey, T. Bürgi, D. Jacquemin, N. Vanthuyne, J. Crassous and N. Avarvari, *Chem. Commun.*, 2017, **53**, 9210–9213.

12 T. R. Schulte, J. J. Holstein, L. Krause, R. Michel, D. Stalke, E. Sakuda, K. Umakoshi, G. Longhi, S. Abbate and G. H. Clever, *J. Am. Chem. Soc.*, 2017, **139**, 6863–6866.

13 J. R. Brandt, X. Wang, Y. Yang, A. J. Campbell and M. J. Fuchter, *J. Am. Chem. Soc.*, 2016, **138**, 9743–9746.

14 H. L.-K. Fu, C. Po, H. He, S. Y.-L. Leung, K. S. Wong and V. W.-W. Yam, *Chem. – Eur. J.*, 2016, **22**, 11826–11836.

15 S. Tanaka, K. Sato, K. Ichida, T. Abe, T. Tsubomura, T. Suzuki and K. Shinozaki, *Chem. – Asian J.*, 2016, **11**, 265–273.

16 T. Ikeda, K. Hirano and T. Haino, *Mater. Chem. Front.*, 2018, **2**, 468–474.

17 X.-P. Zhang, V. Y. Chang, J. Liu, X.-L. Yang, W. Huang, Y. Li, C.-H. Li, G. Muller and X.-Z. You, *Inorg. Chem.*, 2015, **54**, 143–152.

18 M. J. Bryant, J. M. Skelton, L. E. Hatcher, C. Stubbs, E. Madrid, A. R. Pallipurath, L. H. Thomas, C. H. Woodall, J. Christensen, S. Fuertes, T. P. Robinson, C. M. Beavers, S. J. Teat, M. R. Warren, F. Pradaux-Caggiano, A. Walsh, F. Marken, D. R. Carbery, S. C. Parker, N. B. McKeown, R. Malpass-Evans, M. Carta and P. R. Raithby, *Nat. Commun.*, 2017, **8**, 1800.

19 A. Aliprandi, M. Mauro and L. De Cola, *Nat. Chem.*, 2016, **8**, 10–15.

20 (*a*) X.-P. Zhang, T. Wu, J. Liu, J.-X. Zhang, C.-H. Li and X.-Z. You, *J. Mater. Chem. C*, 2014, **2**, 184–194; (*b*) X.-P. Zhang, J.-F. Mei, J.-C. Lai, C.-H. Li and X.-Z. You, *J. Mater. Chem. C*, 2015, **3**, 2350–2357.

21 W. Lu, N. Zhu and C.-M. Che, *Chem. Commun.*, 2002, 900–901.

22 W. Lu, M. C. W. Chan, N. Zhu, C.-M. Che, C. Li and Z. Hui, *J. Am. Chem. Soc.*, 2004, **126**, 7639–7651.
23 (*a*) S.-W. Lai, M. C.-W. Chan, T.-C. Cheung, S.-M. Peng and C.-M. Che, *Inorg. Chem.*, 1999, **38**, 4046–4055; (*b*) W. Sun, H. Zhu and P. M. Barron, *Chem. Mater.*, 2006, **18**, 2602–2610.
24 P. Shao and W. Sun, *Inorg. Chem.*, 2007, **46**, 8603–8612.
25 W. Lu, Y. Chen, V. A. L. Roy, S. S.-Y. Chui and C.-M. Che, *Angew. Chem., Int. Ed.*, 2009, **48**, 7621–7625.
26 S. Y.-L. Leung, A. Y.-Y. Tam, C.-H. Tao, H. S. Chow and V. W.-W. Yam, *J. Am. Chem. Soc.*, 2012, **134**, 1047–1056.
27 *SAINT-Plus, version 6.02*, Bruker Analytical X-ray System, Madison, WI, 1999.
28 G. M. Sheldrick, *SADABS, an empirical absorption correction program*, Bruker Analytical X-ray Systems, Madison, WI, 1996.
29 G. M. Sheldrick, *Acta Crystallogr., Sect. A: Found. Crystallogr.*, 2008, **64**, 112.
30 M. J. T. Frisch, G. W. Trucks, H. B. Schlegel, G. E. Scuseria, M. A. Robb, J. R. Cheeseman, G. Scalmani, V. Barone, B. Mennucci, G. A. Petersson, H. Nakatsuji, M. Caricato, X. Li, H. P. Hratchian, A. F. Izmaylov, J. Bloino, G. Zheng, J. L. Sonnenberg, M. Hada, M. Ehara, K. Toyota, R. Fukuda, J. Hasegawa, M. Ishida, T. Nakajima, Y. Honda, O. Kitao, H. Nakai, T. Vreven, J. A. Montgomery Jr., J. E. Peralta, F. Ogliaro, M. Bearpark, J. J. Heyd, E. Brothers, K. N. Kudin, V. N. Staroverov, R. Kobayashi, J. Normand, K. Raghavachari, A. Rendell, J. C. Burant, S. S. Iyengar, J. Tomasi, M. Cossi, N. Rega, J. M. Millam, M. Klene, J. E. Knox, J. B. Cross, V. Bakken, C. Adamo, J. Jaramillo, R. Gomperts, R. E. Stratmann, O. Yazyev, A. J. Austin, R. Cammi, C. Pomelli, J. W. Ochterski, R. L. Martin, K. Morokuma, V. G. Zakrzewski, G. A. Voth, P. Salvador, J. J. Dannenberg, S. Dapprich, A. D. Daniels, O. Farkas, J. B. Foresman, J. V. Ortiz, J. Cioslowski and D. J. Fox, *Gaussian 09*, Gaussian, Inc., Wallingford CT, 2013.
31 A. Klamt, *J. Phys. Chem.*, 1995, **99**, 2224–2235.
32 T. Bruhn, A. Schaumlöffel and Y. Hemberger, *SpecDis version 1.63*, University of Wuerzburg, Germany, 2015.